THE ARCHIVE OF MECHANICAL ENGINEERING

VOL. LVIII 2011 Number 4

10.2478/v10180-011-0027-1

Key words: channel flow, hydraulic resistance, corrugated walls

JACEK SZUMBARSKI [*], *SLAWOMIR BLONSKI, TOMASZ A. KOWALEWSKI* [**]

IMPACT OF TRANSVERSELY-ORIENTED WALL CORRUGATION ON HYDRAULIC RESISTANCE OF A CHANNEL FLOW

The impact of the transversely-oriented sinusoidal wall corrugation on the hydraulic drag is investigated numerically for the flow through the channel of finite width and with flat sidewalls. The numerical method, based on the domain transformation and Chebyshev-Galerkin discretization, is used to investigate the flow resistance of the laminar, parallel and pressure-driven flow. The obtained results are compared to the reference case, i.e., to the flow through the channel with rectangular cross section of the same aspect ratio. Simple explanation of the gain in the volumetric flow rate observed in the flow through spanwise-periodic channel with long-wave transversely-oriented wall corrugation is provided. In the further analysis, pressure drop in the flows with larger Reynolds numbers are studied numerically by means of the finite-volume commercial package Fluent. Preliminary experimental results confirm the predicted tendency.

List of main symbols

x, y, z	–	spatial coordinates
$\hat{x}, \hat{y}, \hat{z}$	–	dimensionless spatial coordinates
h, L	–	dimension parameters of the channel cross-section
w_P	–	velocity profile of the reference Poiseuille flow
$w_{P,\max}$	–	maximal velocity of the reference Poiseuille flow
W_P	–	dimensionless velocity profile of the reference Poiseuille flow
g_P	–	pressure gradient of the reference Poiseuille flow
G_P	–	dimensionless pressure gradient of the reference Poiseuille flow
Re	–	Reynolds number

[*] *Institute of Aeronautics and Applied Mechanics, Warsaw University of Technology, 24 Nowowiejska St., 00-665 Warszawa, Poland; E-mail: jasz@meil.pw.edu.pl*

[**] *Institute of Fundamental Technological Research, Polish Academy of Science, 5B Pawinskiego St., 02-106 Warszawa, Poland; E-mail:*

q_P – flow rate of the reference Poiseuille flow
W_0 – dimensionless velocity of the flow in the rectangular channel
Q_0 – flow rate of the flow in the rectangular channel
y_b, y_t – functions describing shapes of the bottom and top walls of the corrugated channel
α, S – the wave number and the amplitude of the wall corrugation
W – dimensionless velocity of the flow in the corrugated channel
q – flow rate in the spanwise-periodic channel (no sidewalls), computed for one geometric period of wall corrugation
Q – flow rate in the corrugated channel with sidewalls
ξ, η – spatial coordinates in the computational domain
$\varphi_{i,j}$, $i = 1, .., N_\xi$, $j = 1, .., N_\eta$ – basic functions for the Chebyshev-Galerkin method
ω – Chebyshev weight function

1. Introduction

For the last two decades, laminar flow in channels with corrugated walls has been intensively investigated, both experimentally and numerically. The interest in these flows has been stimulated by various technological applications, where efficiency of mixing processes is of fundamental importance, but flow turbulization is difficult or even undesirable. Numerous examples of this sort come from heat transfer engineering (e.g. compact heat exchangers, cooling of electronic systems), chemical engineering (e.g., biological reactors) and medical engineering (oxygenators, dialyzers). Different passive methods have been proposed with the aim of mixing enhancement in laminar internal flows, in particular different variants of geometrical modification like wall waviness or surface-mounted obstacles and vortex generators. Wall corrugation has attracted particular interest because of its relative technological simplicity. Interestingly, the majority of works have focused on different variants of the longitudinally-oriented, unidirectional wall waviness (Figure 1a), while very few works exist on the internal flow through ducts with transversely-corrugated walls (Figure 1b). The ability of the longitudinal wall corrugation to enhance miffing and heat/mass transfer has been well documented in numerous numerical (e.g. [1,2,3]) and experimental investigations (e.g. [4,5,6]). Transversal wall corrugation was investigated by a few authors in the 90s, but mostly in the context of the skin-friction reduction for turbulent boundary layers and delay of the laminar–turbulent transition.

Recently, Szumbarski [7,8] demonstrated that an appropriate design of transversely-oriented and periodic wall corrugation is capable of destabilizing

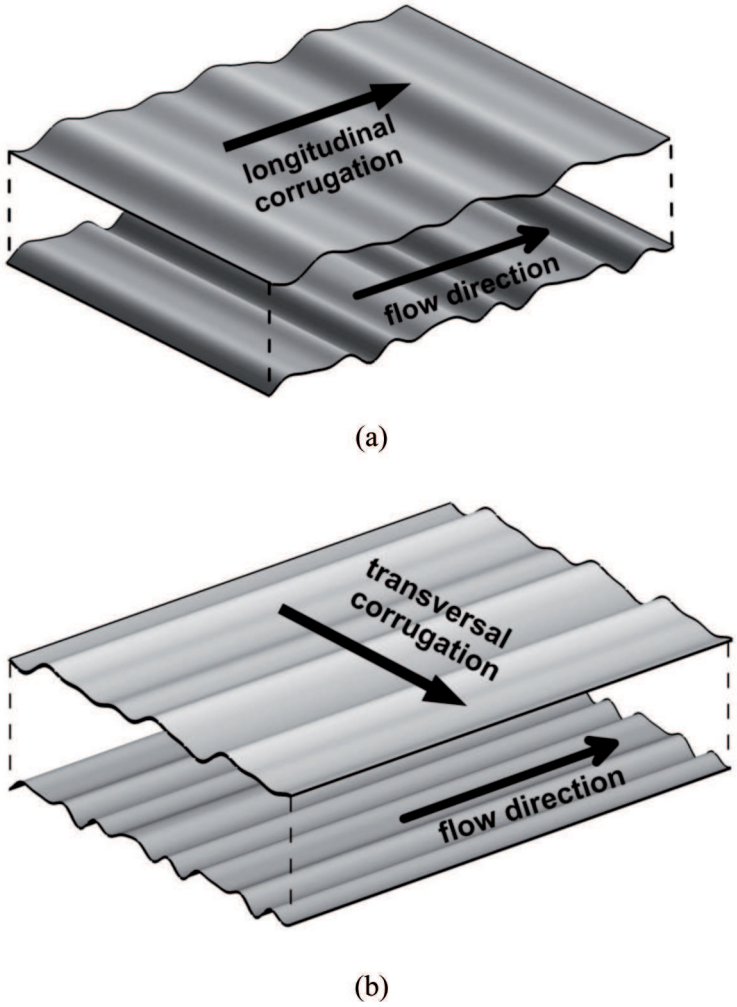

Fig. 1. Channel with bottom and top wall corrugation: oriented longitudinally (a) and oriented transversely (b)

the Poiseuille flow at surprisingly low Reynolds numbers. It was found that using a simultaneous corrugation of both walls the critical Reynolds number appears to be about 58, i.e., it is by two orders of magnitude smaller than the critical Reynolds number of the plain Poiseuille flow. Surprisingly, the transversal wall corrugation which provides the strongest destabilization hardly affects the flow resistance. In other words, the low-Reynolds-number destabilization by the transversely-oriented wall corrugation is obtained "for free", i.e. without excessive hydraulic losses. On the contrary, some small reduction of the hydraulic resistance is possible. Such situation is quite opposite to what is offered by the commonly used variants of the longitudinally-oriented

corrugation or wall-mounted systems of obstacles, where some increase of the flow resistance (sometimes quite significant) is the rule.

Since the analysis presented in [7] and [8] concerned only the idealized case of the unbounded spanwise-periodic flow, it is natural to ask to what extent the properties described above are transferred to more realistic geometry, i.e., the flow through the transversely-corrugated channel closed by two sidewalls. In this work, we focus on the problem of the hydraulic resistance, leaving the much more complicated issue of instability analysis for a separate study [11]. We consider a family of laminar parallel flows of increasing complexity, i.e., ranging from the standard Poiseuille flow up to the destination case, which is the flow through the channel of finite width and with corrugated walls. This family of flows is described in Section 2. Only the destination case of the flow demands the numerical approach, which is the topic of Section 3. The discussion of the obtained results is presented in Section 4. The analysis of flows with larger Reynolds number by means of the finite-volume simulations as well as some preliminary experimental results are presented in Section 5. Finally, short summary and conclusions are presented in Section 6.

2. Hierarchy of the models – from plane Poiseuille flow to the flow in the wavy channel with sidewalls

The analysis of the viscous laminar flow in the channel with finite span and undulated walls can be considered in the reference to simpler cases. The first of such cases is the flow through the channel with rectangular cross section. It means that the span of the channel is finite and the top and bottom walls are flat. On the other hand, one can consider the channel with infinite span, i.e. without sidewalls, and with periodic undulation of the top and bottom walls. Finally, both reference cases can be considered as the modification of the standard Poiseuille flow, i.e. the laminar flow between parallel flat walls, driven by a steady pressure gradient.

2.1. Reference Poiseuille flow

The velocity profile of the stationary, viscous and incompressible flow between two parallel plane walls can be written as

$$w_P(y) = \frac{g_p}{2\mu}\left[h^2 - y^2\right] \tag{1}$$

where the bottom and top walls coincide with the planes $y = -h$ and $y = h$, respectively, the symbol μ denotes viscosity and the constant pressure gradient along z-axis is equal to

$$\frac{dp}{dz} = -g_P < 0 \tag{2}$$

Following standard procedure, we switch to dimensionless description of the flow. To this end, the non-dimensional coordinates are defined as follows

$$\hat{x} = x/h, \quad \hat{y} = y/h, \quad \hat{z} = z/h \tag{3}$$

The non-dimensional velocity profile can be now written as

$$W_P = \frac{w_P(y)}{w_{P,\max}} = 1 - \hat{y}^2 \tag{4}$$

where

$$w_{P,\max} = \frac{g_p h^2}{2\mu} \tag{5}$$

is the maximal velocity attained at the symmetry plane $y = 0$. The corresponding dimensionless pressure gradient can be expressed as

$$G_p = \frac{g_p h}{\rho w_{P,\max}} = \frac{2\mu}{\rho w_{P,\max} h} = \frac{2}{Re} \tag{6}$$

where Re denotes the Reynolds number defined by the formula

$$Re = \frac{w_{P,\max} h}{\nu} \tag{7}$$

The volumetric flow rate of the standard Poiseuille flow, computed per unit length of the channel's span, is equal to

$$Q_P = \int_{-h}^{h} w_P(y)\,dy = \frac{2 g_p h^3}{3\mu} = \frac{4}{3} w_{P,\max} h \tag{8}$$

Thus, the dimensionless flow rate is

$$q_P = Q_P/(w_{P,\max} h) = \frac{4}{3} \tag{9}$$

2.2. Flow in a channel with rectangular cross section

Consider now the laminar pressure-driven and stationary flow in an infinite channel with rectangular cross section (see Figure 2). Let the dimensionless width (or span) of the channel be equal to 2L, i.e. the span-to-height

ratio of the channel section is equal to L. Assume also that the flow is driven by the same pressure drop G_P as in the case of the Poiseuille flow. The corresponding boundary value problem for dimensionless velocity $W_0 = W_0(\hat{x}, \hat{y})$ reads

$$\begin{cases} \hat{\Delta} W_0 \equiv \dfrac{\partial^2 W_0}{\partial \hat{x}^2} + \dfrac{\partial^2 W_0}{\partial \hat{y}^2} = -2 \quad , \quad (\hat{x}, \hat{y}) \in \hat{\Omega} \\ W_0|_{\partial \hat{\Omega}} = 0 \end{cases} \tag{10}$$

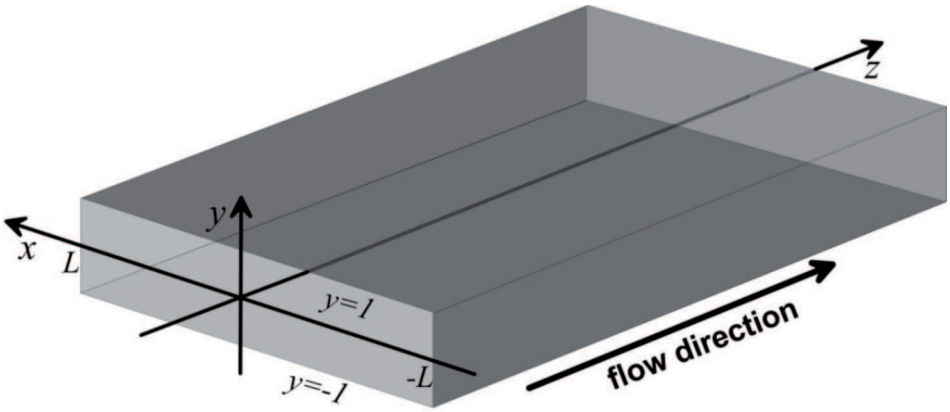

Fig. 2. Channel with rectangular cross section. The aspect ratio of the channel is equal to L

In the following, the hat over the symbols will be omitted – it is understood that all quantities used further on are dimensionless.

The boundary value problem (10) admits the analytical solution in the form of the series (for the derivation, see for instance [9], Ch.8)

$$W_0(x, y) = 1 - y^2 + 4 \sum_{k=1}^{\infty} \frac{(-1)^k}{\delta_k^3} \frac{\cosh(\delta_k x)}{\cosh(\delta_k L)} \cos(\delta_k y) \tag{11}$$

where $\delta_k = \frac{2k-1}{2}\pi$. The velocity distribution (11), computed for $L = 10$, is presented as the contour map in Figure 3. The corresponding flow rate can be expressed as follows

$$Q_0 = Q_0(L) = \frac{8}{3} L \left[1 - \frac{6}{L} \sum_{k=1}^{\infty} \frac{\tanh(\delta_k L)}{\delta_k^5} \right] \tag{12}$$

The effect of the sidewalls on the hydraulic resistance can be evaluated by means of the ratio of the flow rate expressed by the formula (12) to the flow rate of the referential Poiseuille flow computed for the channel spanwise segment of the width equal to $2L$

$$\gamma_0(L) = \frac{Q_0(L)}{2Lq_P} = 1 - \frac{6}{L} \sum_{k=1}^{\infty} \frac{\tanh(\delta_k L)}{\delta_k^5} \tag{13}$$

The plot of the function $\gamma_0 = \gamma_0(L)$ is presented in Figure 4.

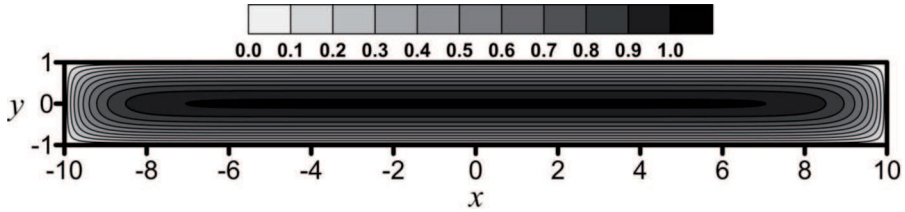

Fig. 3. The contour plot of the velocity of the laminar flow through the rectangular channel. The aspect ratio of the channel's section is $L = 10$

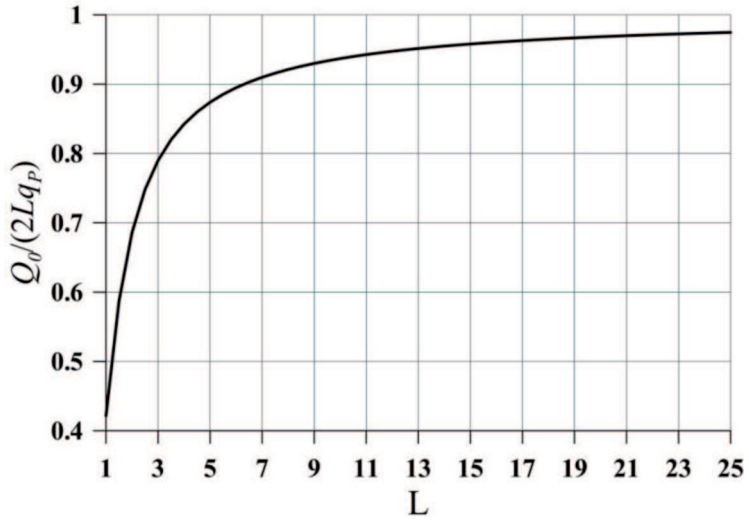

Fig. 4. The ratio of the volumetric flow rate in the rectangular channel to the flow rate of the Poiseuille flow, plotted as the function of the channel section aspect ratio L

2.3. Flow in the channel with transversely-corrugated periodic walls

As it has been already mentioned, the laminar flow through the channel with spanwise-periodic wall corrugation and infinite width (no sidewalls) has been recently studied by Szumbarski in [7] and [8]. One of the main conclusions of this research is that the symmetric sinusoidal wall waviness, given by the formula

$$y_b(x) = -1 - S\cos\alpha x \quad , \quad y_t(x) = 1 + S\cos\alpha x \tag{14}$$

is capable of inducing a low-Reynolds-number destabilization of the Poiseuille flow. The effect of flow destabilization is particularly strong when the wavenumber $\alpha \approx 1$, i.e., when the ratio of the wavelength to the average height of the

channel is close to 3. The velocity of the flow is the x-periodic solution to the Poisson equation (10) in the domain bounded by the wall contours (14) and the vertical lines $x = 0$ and $x = \lambda_x$, where $\lambda_x = 2\pi/\alpha$ is the corrugation wavelength as well as the spanwise period of the flow. This solution has been found for unbounded geometry [7,8] by the semi-analytical and spectrally accurate method based on the concept of immersed boundaries and the least squares formulation. The parametric analysis of the flow resistance has been performed in terms of the corrugation wavenumber α and the amplitude of the corrugation S. It has been observed that the wall corrugation with sufficiently long wavelength (sufficiently small wave number α) is accompanied by the gain in the flow rate, which rises with the amplitude S. Since the area of the cross section of the channel (computed per one wavelength segment of the channel span) is independent of the amplitude S and the pressure gradient driving the flow is fixed, one concludes that the long-wave transversal corrugation actually reduces flow resistance. Justification of this effect has not been given, though.

Here, we will provide a simple mathematical analysis to explain why a long-wave transversal corrugation leads to the reduction of flow resistance with respect to the case of the flat walls (the Poiseuille flow). First, it should be noted that for large wavelengths ($\alpha \to 0$), the local values of the slope of the wall contours are small, even for large corrugation amplitudes. Then, in any section x = const the flow looks very much similar to the two-dimensional Poiseuille flow in the z-direction and confined by the parallel lines (14). Thus, the velocity distribution is well approximated by the following formula

$$W(x, y) \approx (1 + S\cos\alpha x)^2 - y^2 \tag{15}$$

The hydraulic resistance of the flow can be evaluated by referring to the quantity q defined as

$$q = \frac{\alpha}{2\pi}\int_0^{2\pi/\alpha}\int_{y_b(x)}^{y_t(x)} w(x,y)\,dxdy = \frac{\alpha}{\pi}\int_0^{2\pi/\alpha}\int_0^{1+S\cos\alpha x}\left[(1 + S\cos\alpha x)^2 - y^2\right]dxdy \tag{16}$$

which is simply the volumetric flow rate through one segment of the periodic channel. After elementary calculation one arrives at the formula

$$q = \frac{4}{3}\left[1 + \frac{3}{2}S^2\right] = q_P\left[1 + \frac{3}{2}S^2\right] \tag{17}$$

Thus, for sufficiently large corrugation wavelengths, or – equivalently – sufficiently small wavenumber α, the rise of the volumetric flow rate proportional to the square of the corrugation amplitude is expected.

In Figure 5, the ratio q/q_P is plotted versus the amplitude of the wall waviness S and computed for different values of the wave number α using exact formulation given in [7,8]. Obviously, in all cases the flow rate in the corrugated channel increases with the waviness amplitude. The strongest reduction of the flow resistance corresponds to the asymptotic case ($\alpha \to 0$) given by the simple formula (17). One can notice that the plot for $\alpha = 0.1$ practically matches the asymptotic relation. Hence, evidently volumetric flow rate for large corrugation wavelengths becomes solely dependent on the corrugation amplitude S This apparently surprising result can be easily interpreted if one compares flow resistance of the Poisseuille flow calculated for a tube and between two planes.

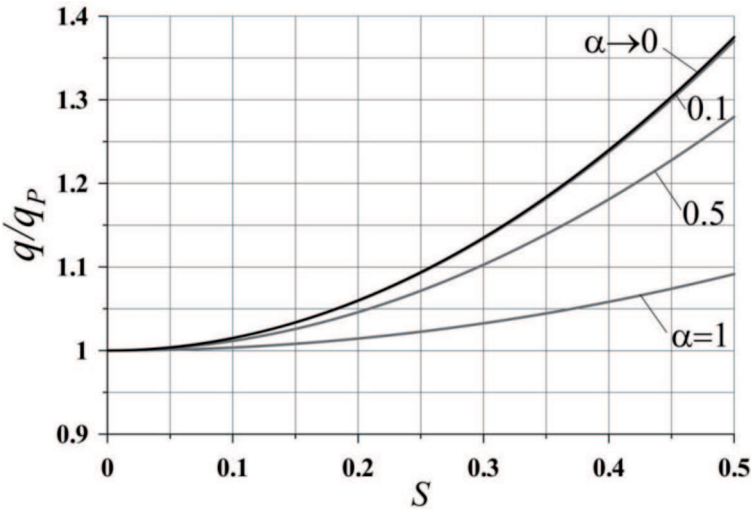

Fig. 5. The ratio of the spanwise density q of the volumetric flow rate in the periodic channel with symmetrically corrugated walls to the density of the flow rate of the Poiseuille flow, plotted as the function of the corrugation amplitude S

2.4. Flow in the wavy channel with the sidewalls

Finally, we consider the flow in the transversely-corrugated channel of a finite width closed by two sidewalls. The width of the channel is equal to $2L$, while the average channel height is equal to 2. The ratio of the width to the average height of the channel section is referred to as the aspect ratio of the channel and it is equal to L. The geometry of the flow domain is depicted in Figure 6.

As before, the Poisson equation with homogeneous boundary conditions should be solved in order to determine the flow velocity W. Since we are interested mostly in the corrugations with large amplitudes, the numerical

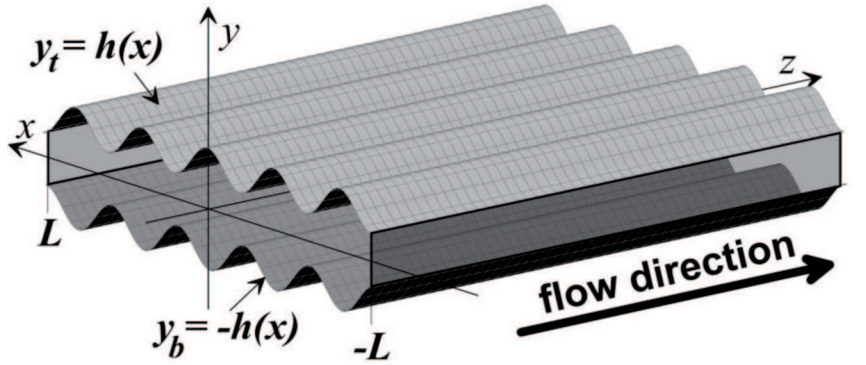

(a)

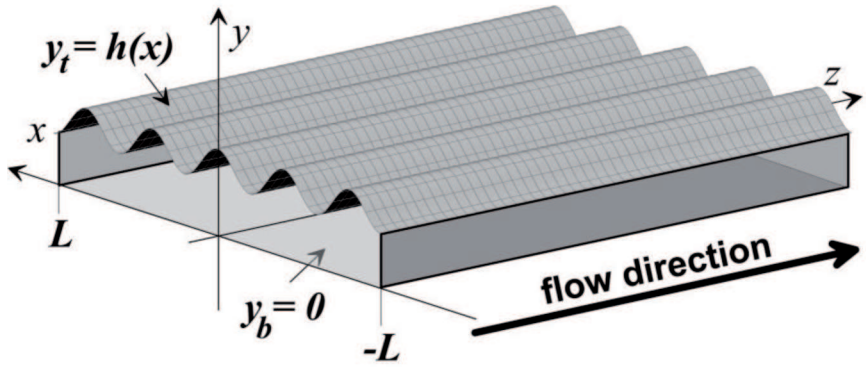

(b)

Fig. 6. Transversely-corrugated channel with flat sidewalls: (a) symmetric corrugation, (b) one-sided corrugation. The aspect ratio of the channel section is $L = 10$

approach based on the application of the immerse boundaries concept is not suitable. Instead, the domain transformation of the cross-section of the wavy channel to the regular square computational domain $[-1, 1]^2$ will be applied. We consider two kinds of wall shapes:

- Symmetric corrugation (Figure 6a)

$$y_t(x) \equiv h(x) = 1 + S\cos(M\pi x/L) = -y_b(x) \tag{18}$$

The corresponding forward and backward domain transformations are defined as

$$\begin{cases} \xi = x/L \\ \eta = y/h(x) = y/[LH(x/L)] \end{cases}, \quad \begin{cases} x = L\xi \\ y = \eta h(L\xi) = L\eta H(\xi) \end{cases} \tag{19}$$

- One-sided corrugation (the top wall is corrugated while the bottom wall remains flat, see Figure 6b)

$$\begin{aligned} y_t(x) &\equiv h(x) = 1 + S\cos(M\pi x/L) \\ y_b(x) &\equiv 0 \end{aligned} \tag{20}$$

The corresponding forward and backward domain transformations are defined as

$$\begin{cases} \xi = x/L \\ \eta = 2y/h(x) - 1 = 2y/[LH(x/L)] - 1 \end{cases}, \quad \begin{cases} x = L\xi \\ y = \frac{1}{2}h(L\xi)(\eta + 1) = \frac{1}{2}LH(\xi)(\eta + 1) \end{cases} \tag{21}$$

In the formulae (20) and (22), we have used the function $H = H(\xi) = h(\xi L)$ defined in the interval $-1 \leqslant \xi \leqslant 1$.

As a result of the domain transformations (19) or (21), the Poisson equation for the flow velocity W transforms to the following differential equation with variable coefficients

$$\tilde{\Delta} W \equiv (\partial_{\xi\xi} - 2\, a_{\xi\eta}\partial_{\xi\eta} + a_{\eta\eta}\partial_{\eta\eta} + a_\eta \partial_\eta)\, W = -2L^2 \tag{22}$$

and the appropriate boundary conditions

$$W(\xi = \pm 1, \eta = \pm 1) = 0 \tag{23}$$

The coefficient functions in the equations (22) are defined as

$$\begin{aligned} a_{\xi\eta} &= a(\eta)\, g_1(\xi) \\ a_{\eta\eta} &= b^2 g_2^2(\xi) + a^2(\eta)\, g_1^2(\xi) \\ a_\eta &= a(\eta)\, [2g_1^2(\xi) - g_3(\xi)] \end{aligned} \tag{24}$$

where

$$g_1(\xi) = H'(\xi)/H(\xi), \quad g_2(\xi) = 1/H(\xi), \quad g_3(\xi) = H''(\xi)/H(\xi), \tag{25}$$

$$b = \begin{cases} 1 & for\ symmetric\ waviness \\ 2 & for\ one-sided\ waviness \end{cases} \tag{26}$$

and

$$a(\eta) = \begin{cases} \eta & for\ symmetric\ waviness \\ \eta + 1 & for\ one-sided\ waviness \end{cases} \tag{27}$$

Finally, the volumetric flow rate can be determined from the formula

$$Q = \int\limits_{\Omega} W\, dxdy = \int_{-1}^{1}\int_{-1}^{1} W(\xi,\eta)\,|J(\xi,\mu)|\, d\xi d\eta = \frac{L^2}{b}\int_{-1}^{1}\int_{-1}^{1} W(\xi,\eta)\, H(\xi)\, d\xi d\eta \tag{28}$$

where symbol J denotes the Jacobian of the domain transformation.

The convenient measure of the flow resistance is the ratio

$$\gamma = Q/Q_0 \tag{29}$$

where Q_0 denotes the volumetric flow rate in the channel with rectangular cross section and the same aspect ratio L (formula (12)).

3. Numerical method

The transformed boundary value problem (22)-(23) can be solved numerically with the use of the spectral approximation [10]. To this aim, the following set of the basic function is defined in the computational domain $[-1,1]^2$

$$\varphi_{i,j}(\xi,\eta) = [T_{i+2}(\xi) - T_i(\xi)]\,[T_{j+2}(\eta) - T_j(\eta)], \quad i = 0,..,N_\xi \quad , \quad j = 0,..,N_\eta \tag{30}$$

In the above, the symbol T_k refers to the Chebyshev polynomial of the order k, and the symbols N_ξ and N_η denote the highest-order polynomials used for transformed coordinates ξ and η, respectively. Thus, the total number of the basic functions (and the dimension of the algebraic problem which follows the discretization procedure) is $M = (N_\xi + 1)(N_\eta + 1)$. Note that each basic function vanishes identically at the boundary of the computation domain.

The solution is sought in the following form

$$W(\xi,\eta) \approx \sum_{i=0}^{N_\xi}\sum_{j=0}^{N_\eta} w_{i,j}\varphi_{i,j}(\xi,\eta) \tag{31}$$

where the coefficients $w_{i,j}$, $i = 0, .., N_\xi$, $j = 0, .., N_\eta$ are to be determined. To this aim, the representation (31) is inserted into the transformed Poisson equation (22) and the following conditions of orthogonality with respect to the finite-dimensional function space spanned by the set of the basic functions (30) are enforced

$$\int_{-1}^{1}\int_{-1}^{1} (\tilde{\Delta} W + 2)\, \varphi_{m,n}\, \omega \, d\xi d\eta = 0 \quad , \quad m = 0, .., N_\xi \quad , \; n = 0, .., N_\eta \tag{32}$$

where

$$\omega = \omega(\xi, \eta) = \left[\sqrt{(1-\xi^2)(1-\eta^2)} \right]^{-1} \tag{33}$$

is the Chebyshev weight function. After simple algebra, the following system of linear equations is obtained

$$\sum_{i=0}^{N_\xi} \sum_{j=0}^{N_\eta} K_{m,n;i,j} w_{i,j} = r_{m,n} \tag{34}$$

where

$$K_{m,n;i,j} = \int_{-1}^{1}\int_{-1}^{1} \varphi_{m,n}\, \tilde{\Delta}\varphi_{i,j} \omega \, d\xi d\eta \quad ; \quad i, m = 0, .., N_\xi \; ; \; j, n = 0, .., N_\eta \tag{35}$$

$$r_{m,n} = -2 \int_{-1}^{1}\int_{-1}^{1} \varphi_{m,n}\, \omega \, d\xi d\eta \quad ; \quad m = 0, .., N_\xi \; ; \; n = 0, .., N_\eta \tag{36}$$

After convenient re-numeration with a single index, the system (34) can be solved by the standard LU factorization routines from the LAPACK library. In all cases considered in Section 4, the choice of $N_\xi = 119$ and $N_\eta = 29$ provides prediction of the volumetric flow rate with the relative error never exceeding 10^{-5}. The corresponding dimension of the linear algebraic system (34) is $N = 3600$.

4. Results

In this Section, the results of the numerical calculations are described. The focus is on the parametric study of the flow resistance. The application of the transversely-oriented wall corrugation leads to the spanwise modulation of the velocity profile. The amplitude of this modulation depends on the wavelength and the amplitude of the wall undulation. Also the average velocity and hence the volumetric flow rate are affected.

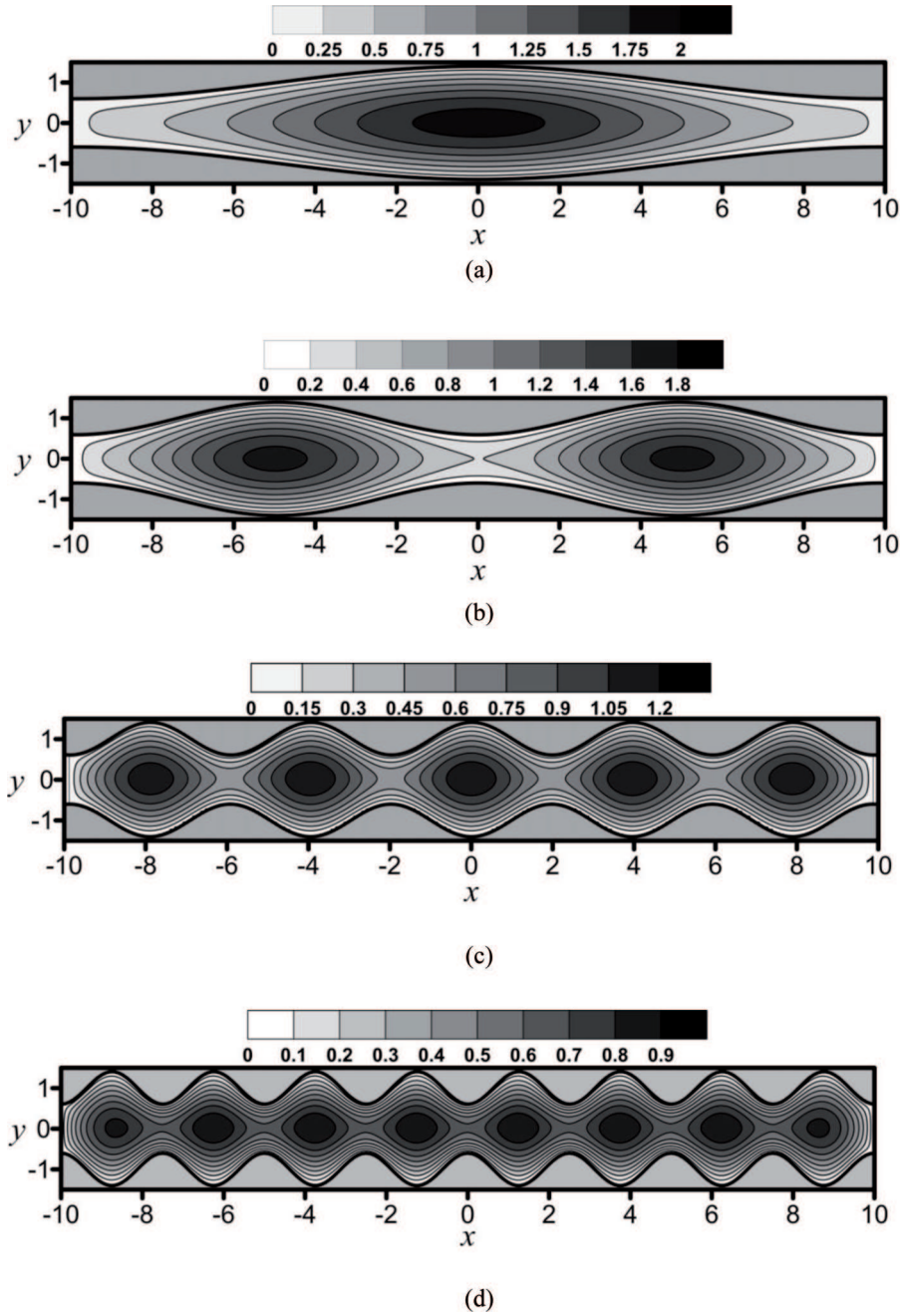

Fig. 7. The contour plots of the velocity distribution computed for the channel of finite width (the aspect ratio $L = 10$) and sinusoidal symmetric corrugation with a different number of the wave periods M: (a) 1, (b) 2, (c) 5 and (d) 8. The amplitude of the corrugation is $S = 0.4$

The typical velocity distributions within the channel section, computed for the case of the symmetric undulation and different number of the wave periods across the channel, are presented in Figure 7. The value of the channel aspect ratio is $L = 10$ and the amplitude of the sinusoidal corrugation (18) is $S = 0.4$, i.e., 20% of the average channel height. The velocity distributions obtained for different numbers of wave lengths across the channel are presented in the form of the contour maps. It is evident that the velocity attains its largest magnitude at the locations of the maximal wall distance, while it is significantly reduced otherwise. This leads to the strong spanwise modulation of the streamwise velocity, especially in the horizontal plane of the channel's symmetry $y = 0$. The velocity distributions computed across the channel span at the symmetry plane are shown in the Fig. 8. For shorter waves ($M = 8$), the overall reduction of the velocity magnitude is clearly visible, which indicates that for such wall geometry the hydraulic drag increases. Similar effect is observed in the case of one-sided corrugation. In the Fig. 9, the contour plots of the velocity are presented. Here, only the top wall is undulated and the amplitude is equal to $S = 0.8$ (40% of the average channel's height). Again, the reduction of the flow rate is observed for short-wave corrugation ($M = 8$).

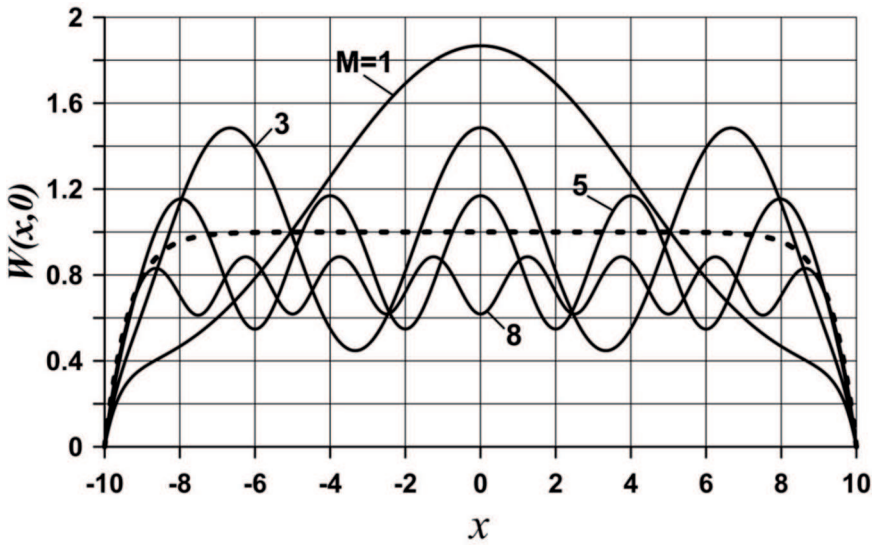

Fig. 8. The velocity profiles computed across the channel in the plane $y = 0$ for the sinusoidal symmetric corrugation (the amplitude is $S = 0.4$), with a different number M of the wave periods. The dashed line corresponds to the velocity of the flow through the rectangular channel. The aspect ratio is equal to 10

The ratio of the volumetric flow rate in the symmetrically corrugated channel to the flow rate in the rectangular channel (with the same aspect

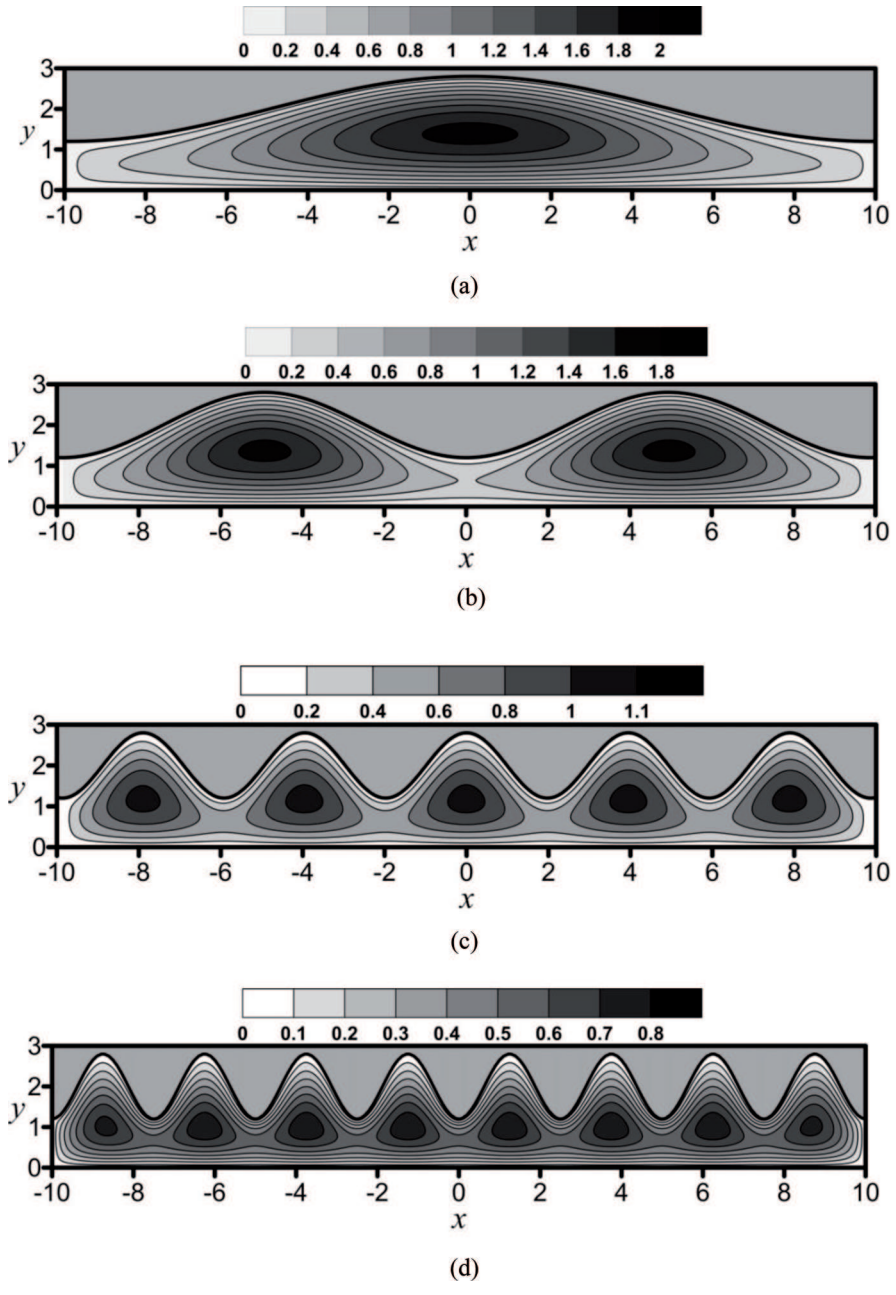

Fig. 9. The contour plots of the velocity distribution computed for the channel of finite width (the aspect ratio $L = 10$) and one-sided corrugation with a different number of the wave periods M: (a) 1, (b) 2, (c) 5 and (d) 8. The amplitude of the corrugation is $S = 0.8$

ratio L and the cross-section area), plotted against the corrugation amplitude S, has been shown in Figures 10a and 10b. Two different aspect ratios of the

channel section have been considered. The results obtained for $L = 10$ are presented in Figure 10a, while the results obtained for $L = 20$ are shown in Figure 10b. Different lines in these plots correspond to different numbers M

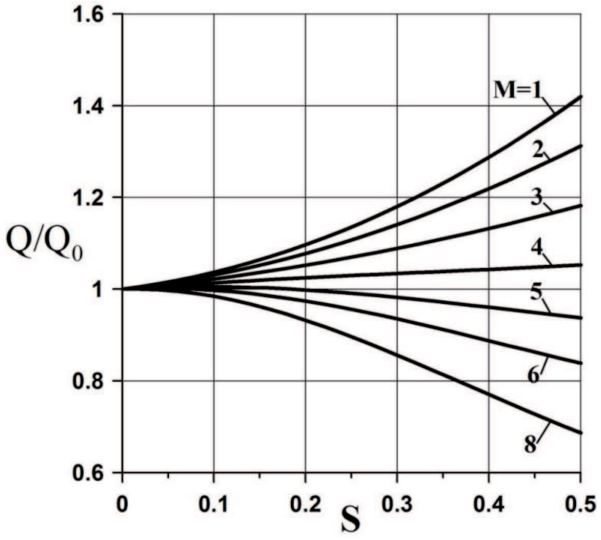

(a)

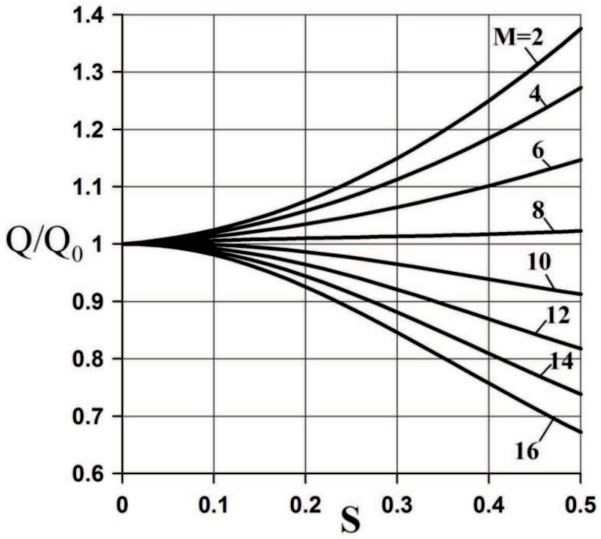

(b)

Fig. 10. The ratio of the volumetric flow rate in the symmetrically corrugated channel to the flow rate in the rectangular channel of the same aspect ratio, computed for different numbers M of the corrugation wave periods and plotted as the function of the corrugation amplitude S. The aspect ratio of the channels is: (a) L = 10, (b) L = 20

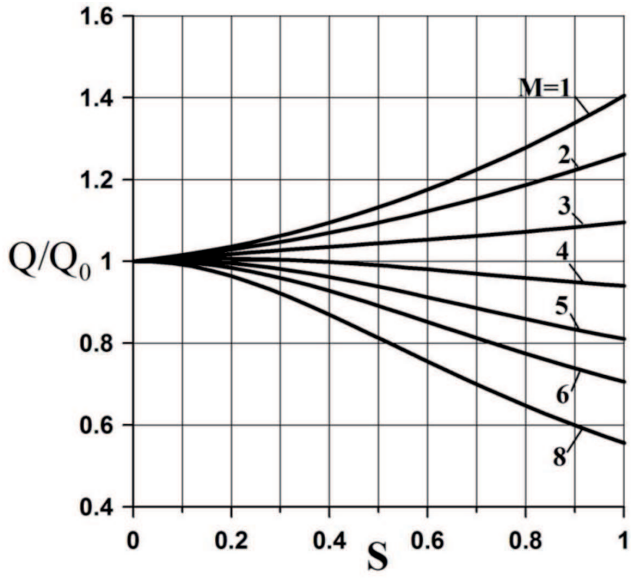

(a)

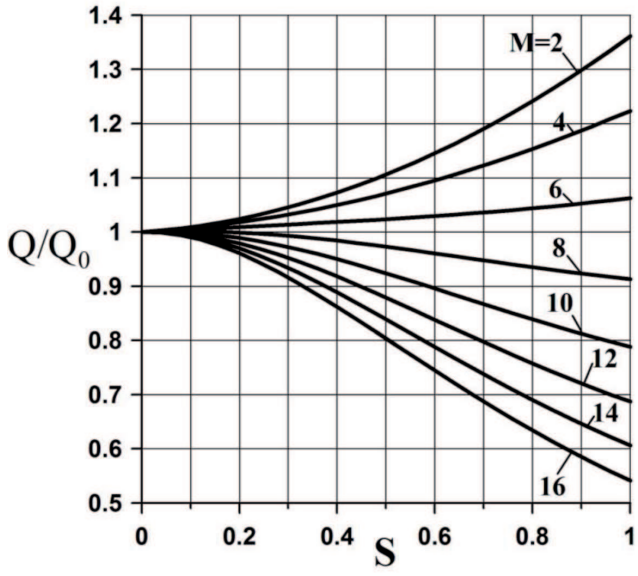

(b)

Fig. 11. The ratio of the volumetric flow rate in the channel with one-sided wall corrugated to the flow rate in the rectangular channel of the same aspect ratio, computed for different numbers M of the corrugation wave periods and plotted as the function of the corrugation amplitude S. The aspect ratio of the channels is: (a) L = 10, (b) L = 20

of the corrugation wavelength across the channel. It is evident that the volumetric flow rate increases when the wavelength of the wall undulation is sufficiently large, i.e., the number M is sufficiently small. Also, there exist a nearly "neutral" values of M for which only minor influence on the flow rate is observed, even for larger corrugation amplitudes. For L = 10, these neutral values are $M = 4$ and $M = 5$, for which the flow resistance is – respectively – either slightly smaller or higher than in the rectangular channel. The results obtained for $L = 20$ indicate that the neutral value of M is 8. Thus, the conclusion is that the symmetric wall corrugation does not affect much the flow resistance as long as the ratio of the corrugation wavelength to the average channel's height is in the range between 2 and 2.5, with a tendency to grow with the aspect ratio of the channel's section. Analogous results obtained for the case of one-sided wall waviness are presented in Figures 11a and 11b. In general, the effect of one-sided wall corrugation on the flow resistance is very much similar to the effect of the symmetric corrugation with the halved amplitude. However, the neutral values of the ratio of the wavelength to the average channel's height are slightly larger and lay in the range between 3 and 4.

5. Results validation

The Finite Volume DNS simulations and preliminary experimental tests were carried out to verify and validate results described in the previous sections, as well as to find out if any gain in the flow resistance can be achieved for higher Reynolds numbers. The experiments were performed in a wavy channel model with removable corrugated wall (Figure 12). Six different corrugation functions were tested for the channel with single corrugated wall. The numerical simulation was performed for the geometry describing as close as possible the experimental configuration. However, it must be pointed out that the numerical model assumes an infinite channel (periodic boundary conditions). Hence, it does not include entry and outlet flow perturbations. DNS for a finite channel length, including all entry and out outlet details, is beyond computational capacity available at the present time.

One of the most striking conclusions formulated in the previous section is the apparent reduction or – at most – rather minor increase in the flow pressure drop introduced by the proposed pattern of the wall waviness (even for large amplitudes). Hence, in the experiment, the pressure drop was measured for the flow of pure water in a wavy channel model with single corrugated wall. The channel was made of metal except upper wall made of glass. Top wall of the channel was flat and transparent, made of glass, to ensure unobscured optical access inside the channel (comp. Figure 12.)

Fig. 12. Experimental model of the wavy channel. The corrugated bottom wall is visible through the top glass wall

The transparent plane wall was necessary to conduct flow structure measurements using microPIV technique (reported elsewhere). The bottom wall was corrugated. The channel design enables easy replacement of the bottom wall, to achieve demanded, different variants of the channel geometry. The measurements were done for 6 configurations of the bottom wall presented in Table 1 and Figure 13. For all these geometries, the length of the test section was 250 mm, width 40 mm and average channel height 2 mm, i.e. aspect ratio was L=20.

Table 1.

Variants of channel geometrical configuration analysed experimentally

No.	Geometry acronym	Top wall	Bottom wall (number of wave periods M and amplitude S)	Sketch (Figure)
1	G_P	flat	flat	13a
2	G_0	flat	M=8, S=0.8 mm	13b
3	G_1	flat	M=8, S=0.6 mm	13c
4	G_2	flat	M=8, S=1.0 mm	13d
5	G_3	flat	M=5, S=0.8 mm	13e
6	G_4	flat	M=10, S=0.8 mm	13f

The pattern of corrugations was selected to cover the optimum predicted by theoretical model, and deviations obtained by increasing and decreasing number of wave periods and/or amplitude of undulation. The same geometry variations were implemented in the numerical simulations performed for the flow of pure water. The simulations were performed using Fluent 12 (Ansys Inc.) numerical package solving unsteady, three-dimensional Navier-Stokes equations on a very fine mesh (10 – 20 millions elements). The numerical domain used in the simulations had to cover full 3D geometry of the physical channel and all spatial scales of the flow structure should

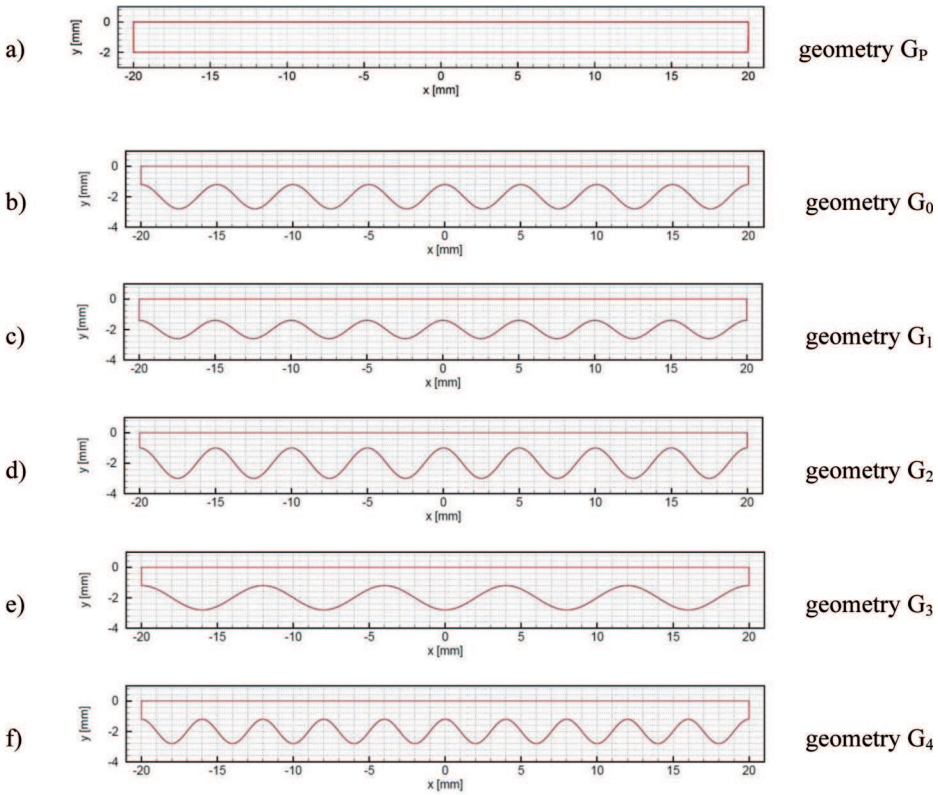

Fig. 13. Schematic drawing of the channel cross-section shape for different geometry variants

be resolved in the computational mesh. To eliminate the influence of entry region, the streamwise periodic conditions was set at the inlet and outlet of the channel (i.e. channel was infinite in the streamwise direction). The non-slip boundary condition was assumed at all other walls.

A constant flow rate of water through the channel model was ensured by precision gear pump (Digital Gear Pump equipped with Suction Shoe Pump Head, Cole Parmer Instrument Co.). The inlet and outlet of the channel were connected with gear pump and water reservoir through 8mm plastic tubes. The minimum and maximum flow rates of the system were about 1 cm^3/s and 70 cm^3/s, respectively, which corresponded to Reynolds numbers of 20 and 1314, respectively. Pressure measurements were done using ultra-precise pressure sensors (class 0.1) at four points located on the symmetry axis of the channel's model. The measurements were performed for 15 different Reynolds numbers, increasing from 36 to 1314, for all variants of the channel geometry.

Figures 14a-14f illustrate the pressure gradient determined as a function of Reynolds number, respectively from numerical (continuous thick line) and

experimental investigations (thinner line with square symbols). The pressure drop predicted by the parallel flow theory has been re-scaled to the physical parameters of the experimental setup – the results of this procedure are shown by thin straight lines.

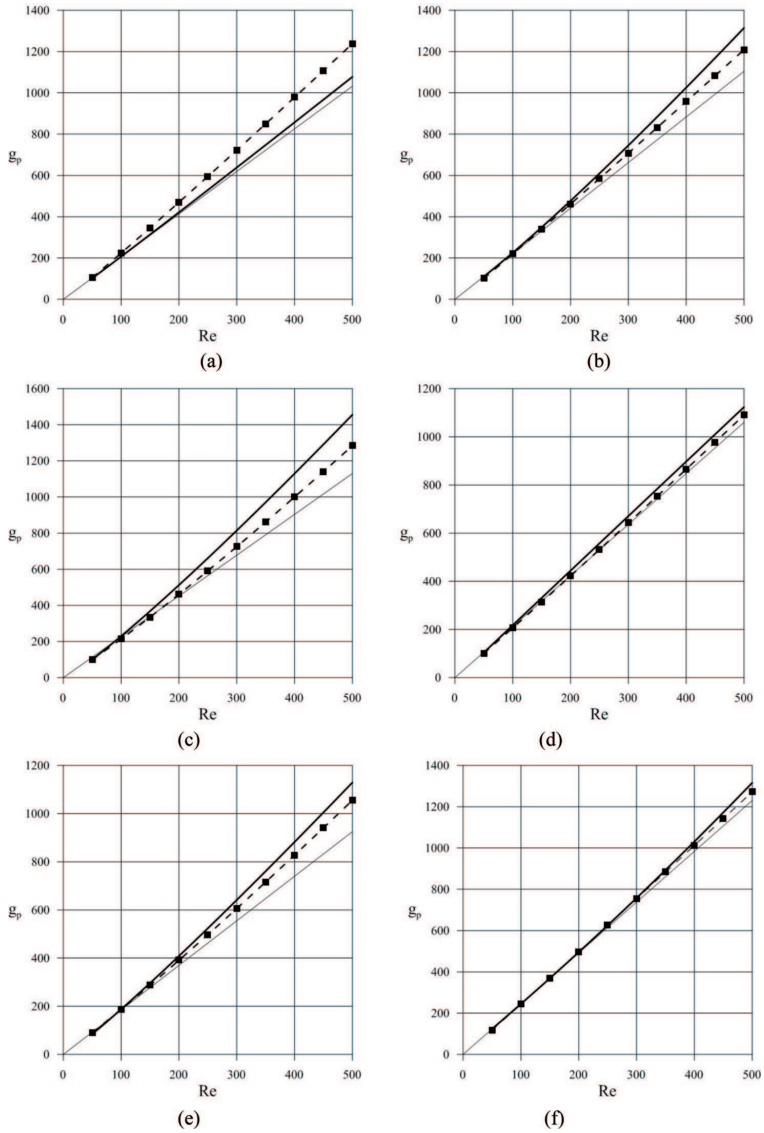

Fig. 14. The pressure drop g_p (measured in Pa/m) plotted versus the Reynolds number for all geometric variants of wall undulation: (a) case G_P (flat walls), (b) case G_0, (c) case G_1, (d) case G_2, (e) case G_3 and (f) case G_4. The variation obtained from CFD simulations (Fluent), linear theory (parallel flow) and experimental measurements are depicted, respectively, by solid thick line, solid thin line and dashed line with square symbols

It can be seen in Figure 14a that, for the channel with rectangular cross section (no wall undulation), denoted here as the case G_p, the predictions of the parallel flow theory and the CFD calculations are in a closed agreement up to the Reynolds numbers around 200. However, experimentally determined pressure drop is larger. At the Reynolds number Re=100, the measured pressure drop is equal to about 224 Pa/m compared to the value around 207 Pa/m obtained from the parallel flow theory and Fluent computations. As the Reynolds number increases, the pressure drops predicted numerically and measured experimentally grow faster than for the one-dimensional flow. For the Reynolds number Re = 500, the measured, computed and predicted by one-dimensional flow theory values of the pressure gradients are, respectively, 1238 Pa/m, 1078 Pa/m and 1033 Pa/m. The substantially larger value of the measured pressure drop can be most likely attributed to the entrance effects and – apparently – the location of the upstream point of pressure probing has been chosen to close to the inlet.

For the flows in the channel with transversely-corrugated bottom wall, the pressured gradient obtained from the parallel flow calculations are pretty close to the values obtained in the CFD calculation as well as those measured experimentally until the Reynolds number does not exceed much the value of 100. For larger values of Re, the pressure drop grows faster than linearly, i.e. the laminar theory underestimates the flow resistance. This effect is not surprising. For each of the considered undulations, the flow with the Reynolds numbers over 100 is expected to become unstable (see [11]) and – eventually – to take a developed three-dimensional form, which is most likely accompanied by increased flow resistance. What is surprising, however, is the fact that for larger corrugation amplitudes, the pressure drop predicted in the Fluent simulations in actually larger than that measured in experiment. At this stage, the authors of this work cannot reliably explain this phenomenon. Another interesting result (and another discrepancy between theory and experiment) can be found once the relative gain in the flow resistance incurred by the wall undulation is considered. Such gain can be measured by taking the ratio of the pressure gradients corresponding to the flow in the corrugated channel to that in the channel with flat walls. The results are presented in Figure 15. Three thick horizontal lines present the ratios predicted by the parallel flow theory, and thinner lines with square symbols illustrate the same ratios measures experimentally. According to this results, the linear theory seems to be too pessimistic for the cases G_2 and G_4, i.e. the actually measured reduction of the flow resistance caused by the bottom wall corrugation is larger. On the other hand, the reduction of the pressure drop expected within the linear theory applied to the case G_3 (characterized

by long-wave undulation with large amplitude) is too optimistic, although the general conclusion about certain flow reduction still remains true.

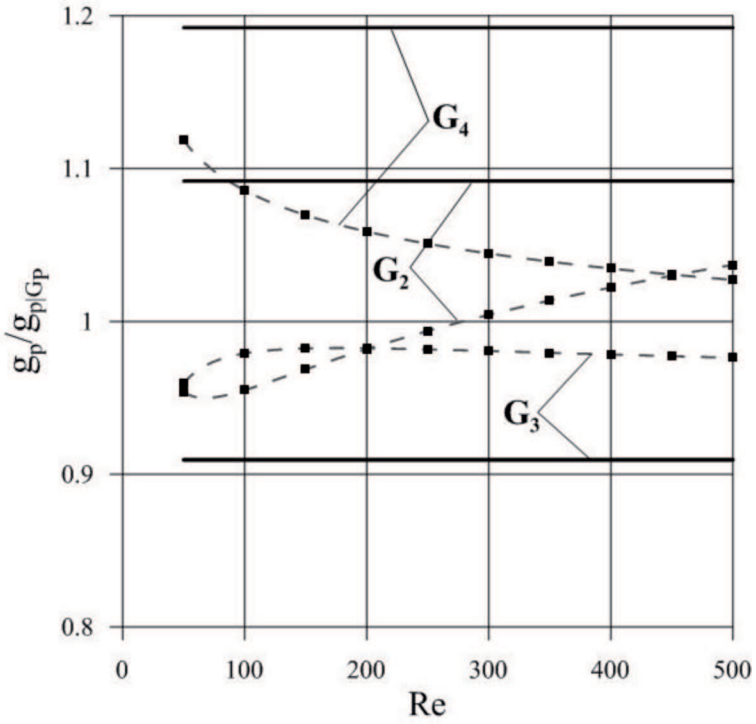

Fig. 15. The ratio of the pressure drop corresponding to selected cases with corrugated wall to the pressure drop in the flow through the reference case G_P (flat walls). The horizontal solid lines correspond to the parallel flow theory, while the dashed lines with square symbols depict the experimental results

The results presented above should be treated as preliminary ones – more investigations are needed to explore fully the potential of transversal wall corrugations as well as to explain the observed peculiarities. Especially, apparent overestimation of the flow resistance obtained in the Fluent calculations definitely requires further study. Clearly, with the periodic inlet /outlet conditions, one would rather expect the opposite behavior. On the other hand, finite length of the physical channel cannot guarantee full development of the transversal flow instabilities, moreover, at the moment we cannot predict how far is this flow from the saturation state present in the numerical results.

Nevertheless, the general trend obtained from experimental and numerical tests confirms that the considered class of the geometric modifications has rather limited influence on the pressure drop in the flows through channels with high aspect ratio. The possibility of slight reduction of the flow resistance has been also confirmed, also in the range of larger Reynolds numbers

beyond the validity of the parallel flow assumption. This is an important conclusion as for most of the engineering configurations of heat exchangers based on the wall corrugation improvement in heat transfer is always at the expense of a noticeable flow pressure lost.

6. Summary and final remarks

It has been demonstrated that transversely-oriented wall corrugation have a great impact on the hydraulic resistance of the laminar flow through the channel. The general rule is that the wall corrugation of large wavelengths leads to drug reduction which is manifested by the increase of the volumetric flow rate driven by a given pressure gradient. On the other hand, short-wave wall corrugation causes reduction of the flow rate. There also exists the neutral range of the corrugation wavelengths in which the flow resistance is hardly affected and basically insensitive to the corrugation amplitude. The obtained results show that such a situation arises when the ratio of the wave length to the average height of the channel assumes values in the range between 2 and 2.5 for symmetric corrugation (19), and between 3 and 4 for the one-sided corrugation (20). This result is of particular interest since this is exactly the range of ratios where the strongest destabilization effect has been found by Szumbarski [7,8] for the unbounded corrugated channel. The systematic stability analysis of the flow through the transversely-corrugated channel with sidewalls [11] confirms these findings for bounded channels. Also, it was confirmed by numerical simulations and preliminary experiments. Computations and measurements show that transverse wall corrugation may be a promising basis for lossless enhancement of mixing efficiency and heat transfer in compact micro-mixers and heat exchangers.

Acknowledgements

This investigation was supported by the Polish Ministry of Science and Education under the project "*Enhancement of the mixing process in micro-flows"*, grant No. N501008733.

Manuscript received by Editorial Board, July 30, 2011;
final version, December 08, 2011.

REFERENCES

[1] Wang G., Vanka S.P.: Convective heat transfer in periodic wavy passages. International Journal of Heat and Mass Transfer, Vol. 38, No. 17, 1995, pp. 3219-3230.

[2] Ghaddar N., El-Hajj A.: Numerical Study of Heat Transfer Augmentation of Viscous Flow in Corrugated Channels. Heat Transfer Engineering, 21, 2000, pp. 35-46.

[3] Niceno B., Nobile E.: Numerical analysis of fluid flow and heat transfer in periodic wavy channel. International Journal of Heat and Fluid Flow, 22, 2001, pp. 156-167.
[4] Nishimura T., Murakami S., Arakawa S., Kawamura Y.: Flow observations and mass transfer characteristics in symmetrical wavy-walled channels at moderate Reynolds number for steady flow. Int. J. Heat and Mass Transfer, 33, 1990, pp. 835-844.
[5] Nishimura T., Kawamura Y.: Three-dimensionality of Oscillatory Flow in a Two-dimensional Symmetric Sinusoidal Wavy-Walled Channel. Exp. Therm. Fluid Sci., 10, 1995, pp. 62-73.
[6] Nishimura T., Kojima N.: Mass transfer enhancement in a sinusoidal wavy-walled channel for pulsatile flow. International Journal of Heat and Mass Transfer, 38, 1995, pp. 1719-1731.
[7] Szumbarski J.: Instability of a viscous liquid flow in a corrugated channel (in Polish, the habilitation thesis). Published by Warsaw University of Technology. Warszawa, 2007.
[8] Szumbarski J.: Instability of viscous incompressible flow in a channel with transversely corrugated walls. Journal of Theoretical and Applied Mechanics, 45, 3, pp. 659-683, 2007.
[9] Chorlton F.: Textbook of Fluid Dynamics. D. Van Nostrand Company Ltd., 1967.
[10] Boyd J.P.: Chebyshev and Fourier Spectral Methods, 2^{nd} Ed. Dover Publication Inc., Minneola NY, 2001.
[11] Szumbarski J., Blonski S.: Destabilization of a laminar flow in a rectangular channel by transversely-oriented wall corrugation. To appear in Archives of Mechanics, Vol. 63, No 4, 2011.

Wpływ poprzecznego pofalowania ścian na opory hydrauliczne przepływu w kanale

S t r e s z c z e n i e

Przedmiotem artykułu jest analiza numeryczna wpływu poprzecznego sinusoidalnego pofalowania ścian na opory hydrauliczne przepływu cieczy lepkiej w kanale. Do wyznaczenia stacjonarnego pola ruchu cieczy lepkiej w kanale posłużono się transformacją obszaru i spektralną metodę Czebyszewa-Galerkina. Obliczone wartości strat ciśnienia porównano z przepływem laminarnym w kanale o ścianach płaskich i przekroju prostokątnym, przy zachowaniu takiej samej wartości stosunku szerokości kanału do jego wysokości. Podano objaśnienie efektu zmiejszenia oporów hydraulicznych w przypadku poprzecznego pofalowania o dużej długości fali. Omówiono również wyniki analizy wpływu pofalowania ścian na straty ciśnienia dla przepływów z większymi liczbami Reynoldsa, uzyskane przy pomocy komercyjnego programu Fluent. Przedstawiono wstępne wyniki badań eksperymentalnych, które potwierdzają zależności otrzymane w modelach numerycznych.